Preprints of the 19th World Congress
The International Federation of Automatic Control
Cape Town, South Africa. August 24-29, 2014

Robust Vertical Plasma Stabilization of the future tungsten divertor configuration of Tore Supra

R. Nouailletas * **E. Nardon** * **S. Brémond** *

* *The authors are with the CEA, F-13108 Saint Paul Lez Durance, France (e-mail: firstname.lastname@cea.fr)*

Abstract: The paper presents the first results of a robust plasma vertical stabilization of TS-WEST: Firstly, a linear MIMO model is identified around an equilibrium point using the free boundary CEDRES++ tokamak equilibrium code. Secondly, from a bode-diagram analysis, the best coil is chosen to feedback control the vertical position of the plasma. Then a H infinity formulation of the problem is used to obtain a robust PI controller. In simulation, supply limitations are taken into account. The controller is validated on CEDRES evolution with 3 tests: stabilization of the plasma position from an offset of 4cm, tracking of the position and robustness to edge localized mode and to transitions between low and high plasma confinement mode.

Keywords: Robust control, unstable, H infinity control, linearization, tokamak,

1. INTRODUCTION

The Tore Supra WEST [1] project aims at the technology testing of one key component of the international leading nuclear fusion ITER project, namely its actively cooled tungsten divertor, for mitigation of the risks related to ITER operation, Blum et al. [2011]. The project includes transforming Tore Supra into an X-point divertor device with elongated cross-section leading to an unstable open-loop plasma vertical position. Passive stabilization studies were first performed in close relation with the overall design of in-vessel components (cf. Ariola and Pironti [2008]) to check that the plasma vertical instability growth rate can be reduced from Alfven growth rates range to in-vessel conducting structures L/R typical growth rates. This was done using a linearized plasma response model computed around the reference equilibrium with the aid of the CEDRES++ free boundary equilibrium code presented by Hertout et al. [2011]. It was found that the upper / lower in-vessel divertor coils, along with additional conducting structures supported from the upper in-vessel divertor coils casing and from the lower baffle, were able to provide all together sufficient passive stabilization, with resulting growth rates in the order of 25s^{-1}. This design study also allowed to specify the main requirements of the power supplies to be used for feedback control, in particular voltage ratings requirements of $50V$ and $10kV/s$, using the "vertical loss of control catch up test" methodology proposed by Humphreys et al. [2009].

This paper is focused on the feedback control design itself. The derivation and open-loop analysis of the linearized plasma response model is discussed in section 2. The control approach is then described in section 3. It includes both the design of a robust low order controller on the unstable part of the plant and the proof of overall stability on the full plant. Sections 4 and 5 are devoted to the testing of the proposed control law against the main foreseen plasma disturbances, such as edge localized modes, transitions between high and low mode, on both linear and non linear plasma response models. Conclusions and outlooks are given in Section 6.

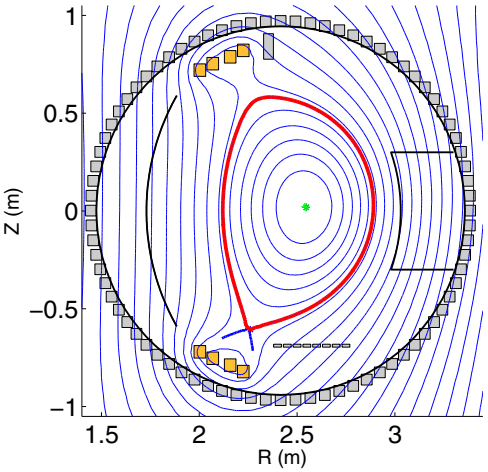

Fig. 1. Cross section of the WEST reference equilibrium used for vertical control studies. The red line represents the plasma boundary, light brown rectangles represent coils and the grey regions correspond to passive conducting structures. The middle green star is the magnetic plasma center that needs to be vertically stabilizated, the x-point is the blue-red cross formed by the plasma boundary.

2. REFERENCE EQUILIBRIUM AND LINEAR MIMO MODEL IDENTIFICATION

In order to design a vertical position control system, a state space model is derived by performing a linearization around a given plasma equilibrium, using the static version of CEDRES++. We consider a lower single null equilibrium with a plasma current $I_p = 600\text{kA}$ and a toroidal field $B_t = 3.9\text{T}$, as shown in Figure 1. The model writes as follows:

[1] Tungsten (W) Environment in Steady-state Tokamak

$$\dot{\Delta I} = A\Delta I + B\Delta u \quad (1)$$

$$I_p\Delta z = C\Delta I + D\Delta u \quad (2)$$

The state of the system is the variation ΔI of the vector I_{PF} of currents in the Poloidal Field (PF) coils (either actual coils or virtual coils representing passive conducting structures, as explained below) around its reference value I^0_{PF}. The input is the vector of voltage variations Δu in the PF coils around the resistive voltage vector associated to I^0_{PF}. The output variable is chosen, for reasons explained below, to be $I_p\Delta z$, where Δz is the variation of the vertical position of the magnetic axis around its reference equilibrium value. We have $A = -(L^*)^{-1}R$ and $B = (L^*)^{-1}$, where R is the vector of coils resistances and L^* is a mutual inductance matrix which takes the effect of the plasma and iron into account: $L^*_{ij} = \frac{\partial \Psi^i_{coil}}{\partial I_j}$. In this equation, Ψ^i_{coil} denotes the magnetic flux intercepted by coil i. Matrix C is a column matrix with coefficients $C_j \equiv \frac{I^0_p \partial z}{\partial I_j}$. Finally, $D = 0$: the equilibrium depends only on coils currents, not voltages.

Using $I_p\Delta z$ as the output rather than simply Δz has two advantages. The first one comes from the fact that the equations describing the system (i.e. the equations of the evolutive version of CEDRES++) are invariant under the following transformation: $I_p \to kI_p$, $I_{PF} \to kI_{PF}$, $\Psi \to k\Psi$, $V \to kV$, assuming that the operator Δ^* is linear neglecting the effect of iron. Thus, a controller designed around an equilibrium corresponding to I_p and I^0_{PF}, using $I_p\Delta z$ as the output, will work exactly in the same way for an equilibrium corresponding to kI_p and kI^0_{PF}, for any k. The second reason is that $I_p\Delta z$ is homogeneous to a magnetic flux variation as could be measured by a flux loop, i.e. it is closer to an experimentally measured quantity than Δz.

Passive conducting structures (grey elements in Figure 1) play a central role in the physics studied here, since in non-static situations they carry induced currents which strongly affect the plasma evolution. In order to derive the linearized model, the passive structures have thus been discretized and treated as fictitious PF coils in the CEDRES++ calculations.

3. ROBUST SYNTHESIS OF A VERTICAL POSITION CONTROLLER

In section 2, a linear model of the plasma vertical position dynamics has been derived. The unstable dynamics of the system imposes feedback control to keep the vertical position z around a desired value. In the case of WEST, the controller gives the variation Δu around the equilibrium point u_0 of the upper divertor coils voltage. This coil was chosen because it is the coil which presents the best sensitivity against the vertical position z, i.e. the bandwidth and the maximal gain of the transfer function is highest (cf. figure 2). Another option may be to couple the upper and lower divertor coils in antiseries, but this solution is more expensive and not needed to fulfill the specifications.

Specifications of power supply are defined by 3 parameters: the delay of the actuator (3.3ms), the saturation voltage (50V) and the voltage rate limiter (10kV/s). The nonlinear behavior of the power supply is not taken into account in the control synthesis, the controller will deal with it a posteriori thanks to a good delay margin and anti-windup system.

From the previous considerations, we obtain a SISO linear model of the vertical position with 44 states corresponding to

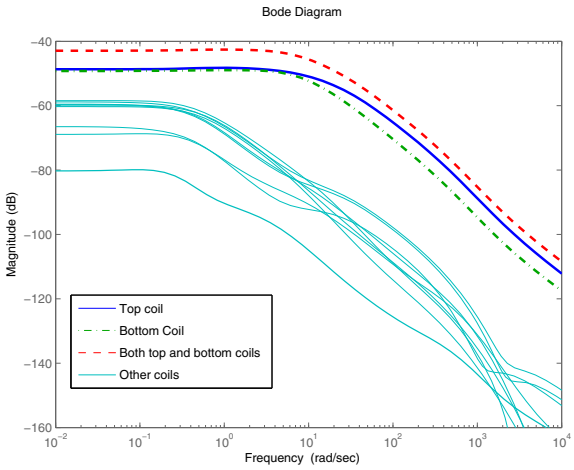

Fig. 2. Bode diagram of the transfer function between Δz and the top divertor coils (solid blue), the bottom divertor coils (dot dashed green), both upper and lower coils connected in antiseries (dashed red) and the other coils (solid cyan)

the currents in the PF coils and virtual coils discretizing the passive conducting structures. To find a controller of small order we propose to reduce first the large size of the model. Using canonical form, the system can be divided into stable and unstable dynamics:

$$\begin{pmatrix} \dot{X}_{st} \\ \dot{X}_{un} \end{pmatrix} = \begin{pmatrix} A_{st} & 0 \\ 0 & A_{un} \end{pmatrix} \begin{pmatrix} X_{st} \\ X_{un} \end{pmatrix} + \begin{pmatrix} B_{st} \\ B_{un} \end{pmatrix} \Delta u$$

$$I_p\Delta z = \begin{pmatrix} C_{st} & C_{un} \end{pmatrix} \begin{pmatrix} X_{st} \\ X_{un} \end{pmatrix} + D\Delta u$$

where X_{st} and X_{un} are respectively the state vectors of the stable and unstable dynamics. The idea of the control synthesis is to find first a controller of low order which stabilizes the unstable dynamics and then to check a posteriori that the full system will keep the right properties.

A robust control approach is used to find a controller $K(s)$ for the system $(A_{un}, B_{un}, C_{un}, D)$. To set the different specifications of the desired closed-loop system, the plant is augmented adding two outputs $z_1(t)$ and $z_2(t)$ (cf. for example the work of Mackenroth [2004]). The plant becomes:

$$\begin{pmatrix} I_p\Delta Z(s) \\ Z_1(s) \\ Z_2(s) \end{pmatrix} = \begin{pmatrix} H(s) & 0 \\ W_1(s)K(s)S(s) & 0 \\ 0 & W_2(s)S(s) \end{pmatrix} \begin{pmatrix} \Delta U(s) \\ I_p\Delta Z_{ref}(s) \end{pmatrix} \quad (3)$$

where $H(s)$ is the nominal plant defined by $(A_{un}, B_{un}, C_{un}, D)$, $S(s)$ is the sensitivity transfer function equal to $(1+KH)^{-1}$. $W_1(s)$ and $W_2(s)$ are weighting transfer functions equal to:

$$W_1(s) = W_1 = G_0 \quad (4)$$

$$W_2(s) = M_{mod}\frac{s + w_c}{s + w_c e_{stat} M_{mod}} \quad (5)$$

W_1 allows us to set the maximal gain of the controller (here a simple constant parameter G_0 is used). For $W_2(s)$, w_c and

e_{stat} set respectively the bandwidth of the closed-loop system and the maximal static error between $I_p\Delta z$ and its reference value $I_p\Delta z_{ref}$. The last parameter M_{mod} is the modulus margin and is used to tune the robustness of the system against model uncertainties.

The robust controller $K(s)$ with input $I_p\Delta z$ and output Δu should minimize the transfer between the outputs z_i and the exogenous input $I_p\Delta z_{ref}$:

$$\min_{\gamma} \| W_1KS \;\; W_2S \|_\infty < \gamma \tag{6}$$

If $\gamma \leq 1$, the transfer function S and KS are respectively bounded by W_1^{-1} and W_2^{-1} for all frequencies.

To solve criterion (6), the augmented system (3) is first written as a generalized LTI system:

$$\begin{pmatrix} \dot{X_a} \\ \hline z_{1,2} \\ I_p\Delta z \end{pmatrix} = \left(\begin{array}{c|cc} A_a & B_1 & B_2 \\ \hline C_1 & D_{11} & D_{12} \\ C_2 & D_{21} & D_{22} \end{array}\right) \begin{pmatrix} X_a \\ I_p\Delta z_{ref} \\ \Delta u \end{pmatrix} \tag{7}$$

with X_a the augmented state including the state vectors of W_1, W_2 and the nominal plant $(A_{un}, B_{un}, C_{un}, D)$. $z_{1,2}$ is the controlled output equal to $\begin{bmatrix} z_1 & z_2 \end{bmatrix}^T$. $I_p\Delta z_{ref}$ is considered as an exogenous input. To find the controller K which minimizes criterium (6), the following result is used:

Theorem 1. (proof presented by Poussot-Vassal [2008])

A dynamical output feedback controller $K : (A_c, B_c, C_c, D_c)$ with n_u outputs and n_y inputs that solves the H_∞ problem is obtained by solving the following LMIs in $(X, Y, \tilde{A}, \tilde{B}, \tilde{C}$ and $\tilde{D})$, while minimizing γ:

$$\begin{pmatrix} M_{11} & (*)^T & (*)^T & (*)^T \\ M_{21} & M_{22} & (*)^T & (*)^T \\ M_{31} & M_{32} & M_{33} & (*)^T \\ M_{41} & M_{42} & M_{43} & M_{44} \end{pmatrix} < 0$$

$$\begin{pmatrix} X & I_n \\ I_n & Y \end{pmatrix} > 0$$

where I_n is the identity matrix of system size n and,

$$\begin{aligned} M_{11} &= A_aX + XA_a^T + B_2\tilde{C} + \tilde{C}^T B_2^T \\ M_{21} &= \tilde{A} + A_a^T + C_2^T \tilde{D}^T B_2^T \\ M_{22} &= YA_a + A_a^T Y + \tilde{B}C_2 + C_2^T \tilde{B}^T \\ M_{31} &= B_1^T Y + D_{21}^T \tilde{B}^T \\ M_{33} &= -\gamma I_{n_u} \\ M_{41} &= C_1X + D_{12}\tilde{C} \\ M_{42} &= C_1 + D_{12}\tilde{D}C_2 \\ M_{43} &= D_{11} + D_{12}\tilde{D}D_{21} \\ M_{44} &= -\gamma I_{n_y} \end{aligned}$$

Then the reconstruction of the controller K is obtained by the following equivalent transformation,

$$\begin{aligned} D_c &= \tilde{D} \\ C_c &= (\tilde{C} - D_cC_2X)M^{-}T \\ B_c &= N^{-1}(\tilde{B} - YB_2D_c) \\ A_c &= N^{-1}(\tilde{A} - YA_aX - YB_2D_cC_2X - \\ &\quad NB_cC_2X - YB_2C_cM^T)M^{-T} \end{aligned}$$

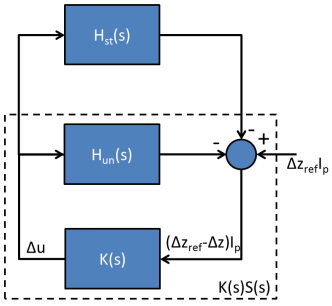

Fig. 3. Control diagram with stable and unstable parts of the plant

where M and N are defined such that $MN^T = I_n - XY$.

Due to the order of the augmented plant, the controller minimizing criterium (6) is equal to:

$$K(s) = \frac{a_2s^2 + a_1s + a_0}{(s - p_0)(s - p_1)}$$

If the maximal static error e_{stat} has been set small enough, the smaller pole (arbitrary chosen equal to p_0) may be approximated by 0. In this case, the controller is equivalent to a PID:

$$K(s) = K_p\left(1 + \frac{1}{T_is} + \frac{T_ds}{\frac{T_d}{a}s + 1}\right)$$

with:

$$\begin{aligned} K_p &= -\frac{1}{p_1}\left(a_1 + \frac{a_0}{p_1}\right) \\ T_i &= -\frac{p_1K_p}{a_0} \\ a &= \frac{a_2}{K_p} - 1 \\ T_d &= -\frac{a}{p_1} \end{aligned}$$

An anti-windup system is added to freeze the integral effect when power supply saturations occur.

Next step is to check if the full order system is still stabilized by the controller $K(s)$. The controller K, the stable part H_{st} and the unstable part H_{un} of the plant are connected following figure 3. Thanks to the theorem of the small gain (cf. Haddad et al. [1993]), the full closed-loop system is stable if the following condition is fulfilled:

$$\|KSH_{st}\|_\infty < 1$$

Finally, the delay margin of the system is calculated. The value is larger than the power supply and data acquisition delay (5.3ms), thus the controller will work.

4. CONTROLLER VALIDATION USING THE LINEAR SISO MODEL

Following the procedure described in the last subsection, a controller K has been synthesized. Table 1 gives the parameters used to tune W_1 and W_2. The minimization of (6) is achieved with $\gamma = 0.95$, the result is a PI controller with $K_p = 1369$ and $T_i = 0.087$s. Figure 4 shows the Bode diagram of the transfer

Table 1. Tuning parameters of W_1 and W_2

Parameters	G_0	w_c	e_{stat}	M_{mod}
Values	65dB	60rad/s	0.01	0.7

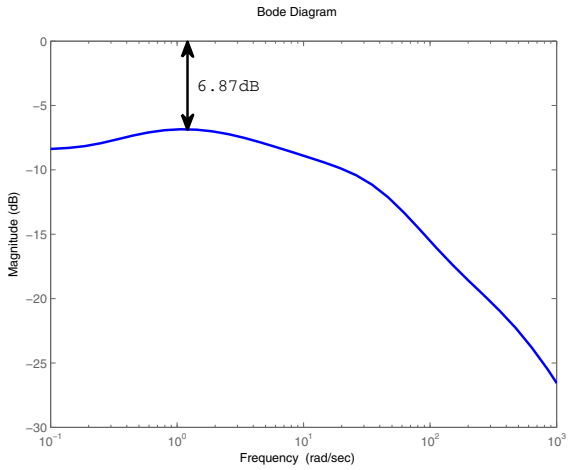

Fig. 4. Bode diagram of the transfer function KSH_{st}

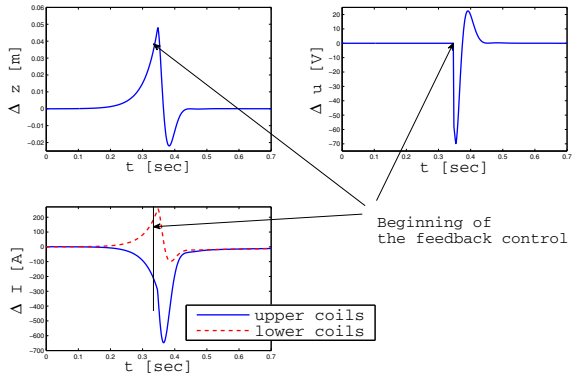

Fig. 5. Stabilization test of the full linear SISO model

function KSH_{st}. The magnitude, less than 0dB, indicates that the full closed loop system will be stable.

To validate the controller in simulation, the following test is done: at the beginning, the system is let uncontrolled and therefore starts diverging. When $|\Delta z|$ becomes larger than 4cm, the feedback control loop is enabled. According to Humphreys et al. [2009], the controller will work in practice if it is able to bring back the plasma to its reference position in this simulation (with the linear model) after a maximal displacement of about 5cm. Figure 5 shows the result: at time $t = 0.3s$ the feedback control begins and stabilizes the plant around the equilibrium point ($\Delta z = 0$). At $t = 3s$, Δz_{ref} is set at 1cm with a ramp of 500ms. The tracking of the position is shown in figure 6. A new equilibrium point is found for the divertor coils current.

The delay margin is equal to 13.5ms which is compatible with the global delay of the closed loop (5.3ms).

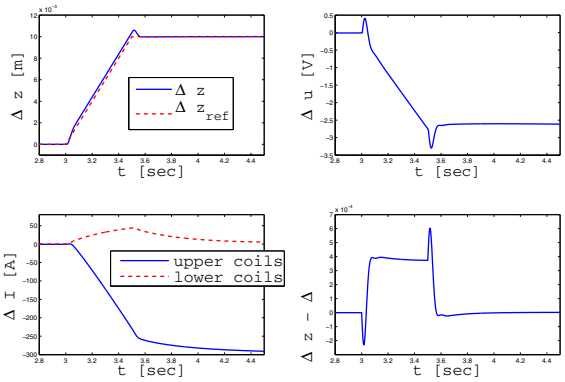

Fig. 6. Test of tracking with the full linear SISO model

5. SIMULATION RESULTS WITH CEDRES EVOLUTION

5.1 Stabilization test

The CEDRES++ equilibrium code has recently been modified to compute dynamic equilibrium by solving together plasma equilibrium equation and circuit equations in coils and passive structures. It will here be referred as CEDRES evolution. The simulation described in section 4 is replayed with this code as the plant. Nonlinear behaviors are added with a delay of 2ms for the acquisition system, a delay of 3.3ms, a saturation voltage of 50V and a rate limiter of 10kV/s for the power supply. The PID controller is discretized with a sample time T_s equal to 2ms. This later is the current one of the Tore Supre PF coils control unit. Results are shown in figure 7 and 8. For the test of stabilization, oscillations are more present with the non-linear plant because the large displacement ($>$ 6cm $\approx$ 15% of the plasma minor radius) before the feedback control phase implies a large difference between behaviors of the nonlinear plant and linear plant which has been used to tune the controller. The linear response is basically valid when the plasma displacements are smaller than 1cm, as found during the derivation of the linear model in section 2. Despite this, the controller is able to stabilize the system thanks to its good properties of robustness against the model uncertainties. For the tracking test, the system is able to follow the vertical position reference with only a small overshoot. Due to the small variation of Δz, the nonlinear plant is still more or less close to the linear plant and the difference between the linear and nonlinear simulations on Δu and ΔI are smaller than in the stabilization test.

5.2 Robustness against plasma disturbance

The plasma equilibrium can be disturbed by many things. Here, we consider three types of disturbances. The first one is caused by a series of periodic edge localized modes (ELMs) and the second one by a transition from low plasma confinement mode (L mode) to high plasma confinement mode (H mode). The last one is the opposite transition from L mode to H mode.

An ELM causes a large and fast drop of the plasma kinetic pressure (typically in 200μs) which later recovers approximately linearly up to its initial state, at which point the next ELM is triggered (for more details see the work of Wesson [1997] or Loarte et al. [2003]). The process repeats itself with a frequency of typically 50Hz for a machine like TS-WEST. ELMs are due

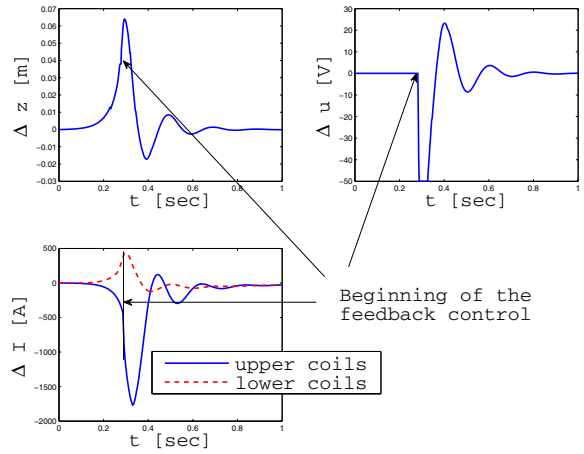

Fig. 7. Stabilization test of the non linear plant (CEDRES evolution)

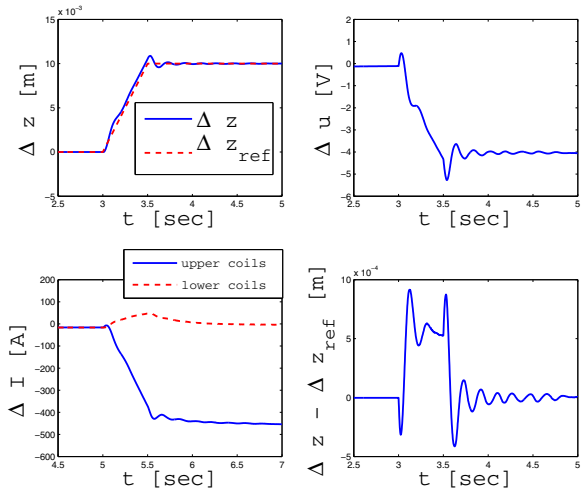

Fig. 8. Test of tracking with the non linear plant (CEDRES evolution)

to a magnetohydrodynamic instability which releases a significant fraction of the plasma thermal energy to the divertor targets and the wall.

LH (from L mode to H mode) and HL (from H mode to L mode) transitions modify also equilibrium via the pressure (or poloidal beta), which is roughly halved during the transition, Wesson [1997].

The three cases represent a disturbance in the equilibrium (which is cyclic in the case of the ELMs), which the vertical control system has to overcome. In the case of the ELMs and of LH transition, the controller should be able to keep the X-point away from the target plates of the divertor, otherwise the H mode may be lost. On the other hand, in the case of the HL transition, the main goal is to avoid a loss of vertical control, which would result in a so-called vertical displacement event ending up presumably in a plasma disruption.

In practice, for ELMs, a drop of 10% of the poloidal beta β_p is assumed over 2ms followed by a linear recovery with

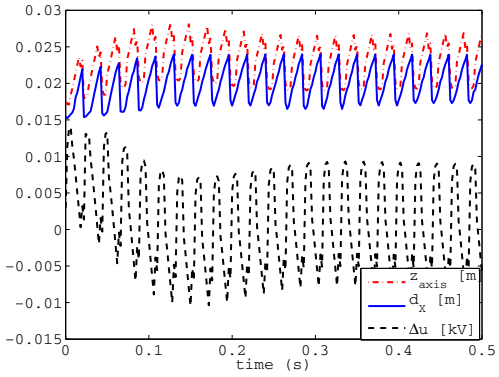

Fig. 9. Test of robustness against repetitive ELMs ($I_p = 1MA$)

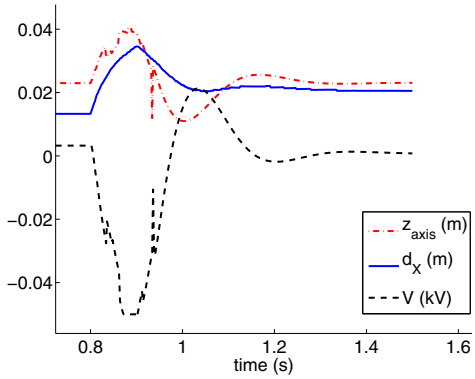

Fig. 10. Test of robustness against L to H mode transition ($I_p = 1MA$, transition time at $t = 0.8$s)

a frequency of 50Hz, cf. Hertout et al. [2011], Loarte et al. [2003]. For the LH transition, β_p is increased of 100% in $100ms$, Wesson [1997]. For HL transition, β_p is dropped of 50% in 100ms to recover L mode plasma confinement.

A simulation of vertical stabilization in presence of ELMs is shown in figure 9: the system reaches a periodic disturbed state; however the distance d_x between the x-point and the divertor stays positive. This is essential in order to avoid loosing the H-mode.

For LH transition, the X-point is kept away from the target plates of the divertor, cf. figure 10. It means that the H mode can be achieved a priori without special tuning of the controller and PF coils values.

The HL transition is shown in figure 11. The controller successfully brings back the plasma to its initial position after the transition at $t = 1.5$s. The x-point reaches the divertor during around 55ms. In this case, the issue of keeping the H-mode confinement doesn't existed and the heat flux see by the divertor during this transient phase is in principle small enough to not damage it. The quantity of impureties that penetrate the plasma and the consequences on the plasma ending needs to be investigated.

6. CONCLUSION AND FUTURE WORKS

The future tungsten divertor configuration of Tore Supra aims at achieving diverted and thus elongated plasmas configurations. This type of shape is vertical unstable and needs to be feedback

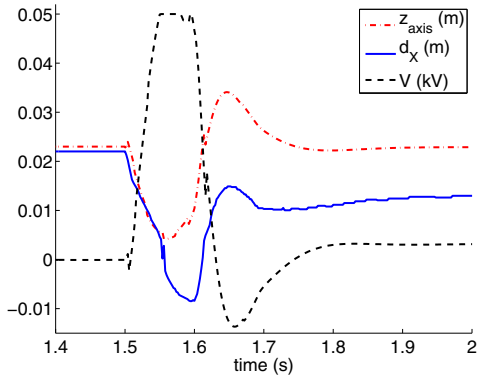

Fig. 11. Test of robustness against H to L mode transition ($I_p = 1MA$, transition time at $t = 1.5$s)

controlled. In this paper, we have identified a LTI model around a reference equilibrium using the free-boundary CEDRES++ tokamak equilibrium code. Then a robust approach has been used to synthesize a PI controller to control the unstable dynamics. Firstly, the control law is validated on the LTI model and then on the CEDRES evolution code. Robustness against ELM disturbance, LH and HL transitions is checked. The end result is that the proposed controller is enough efficient to operate in H mode and handle the different transitions.

Next step will be to apply the presented control synthesis approach to a MIMO case: the control of the gaps between the vessel wall and the plasma edge. These quantities are built in real-time by a dedicated algorithm which uses raw data coming from the magnetic diagnostic, Blum et al. [2013]. This work will allow studying the transition between limiter configuration and divertor configuration of the plasma at the beginning and at the end of the pulse.

REFERENCES

Ariola, M. and Pironti, A. (2008). *Magnetic control of tokamak plasmas*. Advances in Industrial Control series ISSN 1430-9491, Spinger-Verlag.

Blum, J., Boulbe, C., and Faugeras, B. (2011). Reconstruction of the equilibrium of the plasma in a tokamak and identification of the current density profile in real time. *Journal of computational physics*.

Blum, J., Boulbe, C., and Faugeras, B. (2013). Equilibrium reconstruction from discrete magnetic measurements in a Tokamak: the Equinox code. *8th Workshop on Fusion Data Processing, Validation and Analysis*, Belgium, 2013.

Haddad, W., Collins, E., and Bernstein, D. (1993). Robust stability analysis using the small gain, circle, positivity, and popov theorems: a comparative study. *IEEE Transactions on Control Systems Technology*, 4, 290–293.

Hertout, P., Boulbe, C., Nardon, E., Blum, J., Bremond, S., Bucalossi, J., Faugeras, B., Grandgirard, V., and Moreau, P. (2011). The cedres++ equilibrium code and its application to iter, jt-60 sa and tore supra. *Fusion Engineering and Design*, 86, 1045–1048.

Humphreys, D., Casper, T., Eidietis, N., Ferrara, M., Gates, D., Hutchinson, I., Jackson, G., Kolemen, E., Leuer, J., Lister, J., LoDestro, L., Meyer, W., Pearlstein, L., Portone, A., Sartori, F., Walker, M., Welander, A., and Wolfe, S. (2009). Experimental vertical stability studies for iter performance and design guidance. *Nuclear Fusion*, 49, 115003.

Loarte, A., Saibene, G., Sartori, R., Campbell, D., Becoulet, M., Horton, L., Eich, T., Herrmann, A., Matthews, G., Asakura, N., Chankin, A., Leonard, A., Porter, G., Federici, G., Janeschitz, G., Shimada, M., and Sugihara, M. (2003). Characteristics of type i elm energy and particle losses in existing devices and their extrapolation to iter. *Plasma Phys. Control. Fusion*, 45, 1549–1569.

Mackenroth, U. (2004). *Robust control systems: theory and case studies*. Springer.

Poussot-Vassal, C. (2008). *Robust Linear Parameter Varying Multivariable Automotive Global Chassis Control*.

Wesson, J. (1997). *Tokamaks, second edition*, chapter 4. The oxford engineering science series.